International Journal of Science and Research Archive
eISSN: 2582-8185
Cross Ref DOI: 10.30574/ijsra
Journal homepage: https://ijsra.net/

(RESEARCH ARTICLE)

Check for updates

Optimizing methane direct utilization: The advanced $Sr_2CoMoO_{6-\delta}$ anode

Seyed Mostafa Nasrollahpour Shirvani [1], Amin Nakhi [2], Amirmohammad Karimi [3] and Mostafa Mobli [4,*]

[1] *Department of Mechanical Engineering, Babol Noshirvani University of Technology, Babol, Iran.*
[2] *Nanotechnology and Advanced Materials Department, Materials and Energy Research Center, Karaj, Iran.*
[3] *Department of Chemical Engineering, Azad University, Tehran, Iran.*
[4] *Department of Mechanical Engineering, University of South Carolina, Columbia, United States.*

International Journal of Science and Research Archive, 2023, 10(02), 607- 617

Publication history: Received on 22 October 2023; revised on 01 December 2023; accepted on 03 December 2023

Article DOI: https://doi.org/10.30574/ijsra.2023.10.2.0987

Abstract

The rising global demand for energy, combined with environmental concerns linked to conventional energy sources, has spurred interest in sustainable and diverse alternatives. This study focuses on enhancing the efficiency of energy conversion devices, specifically solid oxide fuel cells (SOFCs). While conventional Ni/YSZ cermet anodes show promise for the anode of SOFCs, they face challenges, prompting exploration into alternative materials such as $Sr_2MMoO_{6-\delta}$ (M= Fe, Co, Ni) perovskites. This work investigates the electro-oxidation of methane on $Sr_2CoMoO_{6-\delta}$ (SCM) anodes and explores the impact of Pd infiltration as a metallic element together with $LaFe_{0.6}Co_{0.4}O_3$ and as a dopant in $LaFe_{0.58}Co_{0.37}Pd_{0.05}O_{3-\delta}$ (LFCP). Experimental results reveal improved performance, reduced polarization resistance, and enhanced catalytic activity in SCM anodes impregnated with LFCP, attributed to the homogeneous dispersion of nanoparticles within the anode structure. The study provides insights into optimizing SOFC anode materials for efficient methane electro-oxidation, with potential applications in clean energy technologies.

Keywords: Solid Oxide Fuel Cell; Anode Electrode; SCM; Electrochemical Impedance Spectroscopy; Methane Oxidation; Impregnation

1. Introduction

The escalating global demand for energy, coupled with the considerable environmental repercussions associated with conventional energy sources, has stimulated the exploration of sustainable and diverse energy alternatives [1-9]. A central focus of this endeavor centers on enhancing the efficiency of energy conversion devices, specifically emphasizing solid oxide fuel cells (SOFCs) [10-18] and batteries [19-21]. SOFCs, recognized as highly efficient energy conversion devices, generate electricity through the electrochemical reaction of gaseous fuels, with hydrogen and its carriers serving as the primary fuel sources [22-29]. Notably, SOFCs distinguish themselves from other fuel cell types by their capability to directly utilize hydrocarbon fuels through internal reforming processes [30-35]. Methane, being the simplest hydrocarbon with a singular carbon atom in its structure, stands out for its absence of a robust C–C bond, facilitating reforming processes for direct integration within SOFCs [32, 36-39]. Furthermore, methane boasts a favorable hydrogen-to-carbon ratio, contributing a substantial number of hydrogen molecules for the anode electrode in SOFCs.

In conventional SOFC configurations, Ni/YSZ ($Zr_xY_{1-x}O_2$) cermet serves as a promising material for the anode electrode, offering advantages such as low impedance in the presence of hydrogen and catalytic activity for methane steam reforming [40-47]. However, this material presents certain drawbacks, notably low redox stability, and heightened catalytic activity leading to coking and sulfur poisoning when utilized with hydrocarbon fuels [48-50]. To address these challenges, alternative ceramic anodes, including double perovskite materials such as $Sr_2Mg_{1-x}Mn_xMoO_{6-\delta}$ [51] and

* Corresponding author: Mostafa Mobli.

$Sr_2Fe_{1.4}Ni_{0.1}Mo_{0.5}O_{6-\delta}$ [16, 52], lanthanum chromate based perovskites (e.g. (La,Sr)(Cr,Mn)$O_{3-\delta}$) [26], and strontium titanate based perovskites (e.g. (La,Sr)(Ti)$O_{3-\delta}$) [53], have demonstrated promising properties for application in SOFC anodes.

$Sr_2MMoO_{6-\delta}$ (M=Co, Ni) perovskites have garnered attention as a promising anode material owing to their notable tolerance to carbon and sulfur, as well as their stability in redox and thermal cycling [54]. Huang et al. [55] examined the behavior of $Sr_2CoMoO_{6-\delta}$ (SCM) anode during methane utilization as a fuel, revealing a maximum power density of approximately 0.527 W cm^{-2} at 900 °C, comparable to that of the Ni/YSZ-based anode in wet H_2. Dos Santos-Gomez et al. [54] reported a polarization resistance of 6.5 Ω cm^2 at 750 °C for 5%H2-Ar oxidation reaction on SCM anode, with no observed carbon deposition following electrochemical impedance spectroscopy. Nevertheless, there remains a need for enhancement in the conductivity and catalytic activity of ceramic anodes such as SCM [56].

A well-established and effective methodology for improving the performance of SOFC electrodes involves the impregnation of nanoparticles composed of oxides or precious metals into the electrode matrix [26, 41, 57-60]. Rath et al. [61] conducted a comparative analysis of the $Sr_2FeMoO_{6-\delta}$ (SFM) anode infiltrated with Pd against Co-Ni-Mo (0.1:5:1 molar ratio, CNM) nanoparticles for operation in humidified hydrogen. Their findings revealed that the Pd-impregnated SFM anode exhibited a slightly higher electrode polarization resistance (0.087 Ω cm^2) in comparison to the CNM-impregnated SFM (0.060 Ω cm^2). Recent investigations have explored $LaFe_{0.7}Co_{0.3}O_{3-\delta}$ and $LaFe_{0.67}Co_{0.3}Pd_{0.03}O_{3-\delta}$ perovskites as symmetric electrode materials for SOFC [62], demonstrating commendable electro-catalytic activity for both hydrogen oxidation and oxygen reduction reactions. Specifically, at 750 ºC, the power density of symmetric $LaFe_{0.7}Co_{0.3}O_{3-\delta}$/$Sm_{0.2}Ce_{0.8}O_{1.9}$ (SDC) and $LaFe_{0.67}Co_{0.3}Pd_{0.03}O_{3-\delta}$/SDC was reported as 291 and 535 mW cm^{-2}, respectively. Additionally, Pd doping was observed to significantly enhance the catalytic activity of $LaFe_{0.7}Co_{0.3}O_{3-\delta}$ for H_2 oxidation reaction.

In the present study, the electro-oxidation of methane on the SCM anode was systematically investigated. To enhance the performance of the SCM electrode, the impact of Pd infiltration, along with solution of $LaFe_{0.6}Co_{0.4}O_3$ (LFC+Pd) and doped-in $LaFe_{0.58}Co_{0.37}Pd_{0.05}O_{3-\delta}$ (LFCP) perovskite structures, was thoroughly explored. The mechanism of the methane oxidation reaction on the promoting anode was investigated using comprehensive electrochemical measurements, and both pure and impregnated samples were subjected to microstructural analysis.

2. Materials and Methods

In order to manufacture electrolyte pellets, we utilized an 8 mol % yttria-stabilized zirconia (YSZ) material sourced from Tosoh in Japan. This material underwent a cold pressing process and was subsequently sintered at a temperature of 1400 °C for a duration of 6 hours. As a result, the obtained pellets exhibited an approximate diameter of 22 mm and a thickness of 0.9 mm. To function as the counter electrode with a surface area of 0.5 cm^2, a layer of Pt paste was applied specifically to the central region of the YSZ pellets. In addition, a reference electrode was implemented in the form of a ring. Both the counter and reference electrodes were subjected to an air environment and heated at 850 °C for a period of 1 hour.

To fabricate the anode electrode, $Sr_2CoMoO_{6-\delta}$ (SCM) powder was mixed with an appropriate quantity of Ink Vehicle to create a well-suited SCM slurry. This slurry was applied to the opposite side of the counter electrode and subjected to sintering at a temperature of 1200 °C for a duration of 1 hour under ambient air conditions. Following the sintering process, the anode exhibited a surface area of 0.5 cm^2 and a thickness of 35 µm.

The preparation of $LaFe_{0.6}Co_{0.4}O_3$ (LFC) and $LaFe_{0.58}Co_{0.37}Pd_{0.05}O_3$ (LFCP) solutions for impregnation involved a sequential process. First, a stoichiometric mixture of $La(NO_3)_3{\cdot}6H_2O$, $Fe(NO_3)_3{\cdot}9H_2O$, $Co(NO_3)_2{\cdot}6H_2O$, and $Pd(NO_3)_2$ (all sourced from Merck, Germany) in specific ratios of 1:0.6:0.4:0 for LFC and 1:0.58:0.37:0.05 for LFCP, was prepared using an aqueous solution. The concentration of both LFC and LFCP solutions was maintained at 0.3 M. To serve as a complexing agent, ethylene glycol (EG) was added to the solution in a ratio of 2.4:1 M. Subsequently, a single drop of either LFC or LFCP solution was carefully applied to the surface of a SCM anode. After impregnation, the electrode surface was gently wiped with a tissue and left to dry in ambient air. The impregnated cells were then subjected to heating at 900 °C for a duration of 2 hours under ambient air conditions. In order to compare the catalytic impact of palladium (Pd) as a dopant within the perovskite structure versus its role as an individual metallic particle adjacent to a perovskite, a single drop of $Pd(NO_3)_2$ solution with a concentration of 0.3 M was trickled onto the surface of the electrode containing LFC, following the same drying procedure.

The drying of LFC and LFCP solutions was carried out in an oven and subsequently subjected to calcination at a temperature of 900 °C for a duration of 2 hours in an ambient air environment, following the method employed by

Rostaghi Chalaki et al. [26] for the calcination of LFC and LFCP. The phase composition of the calcined LFC and LFCP powders was evaluated using X-ray diffraction (XRD) analysis conducted at room temperature. A Philips PW 1730 instrument equipped with Cu-Kα radiation (λ=1.5406 Å) was utilized, covering a range of 20°<2θ<80° with a step size of 0.02°. To assess the microstructure of the impregnated SCM anodes, field emission scanning electron microscopy (FESEM) was employed using a TESCAN MIRA3 instrument.

Electrochemical measurements were conducted using a three-electrode configuration. To serve as a current collector, platinum paste was applied onto the surface of the anode electrode, while platinum wires were selected as the current leads. Methane was employed as the fuel during the experiments. The counter and reference electrodes were exposed to the surrounding atmosphere. Prior to the initiation of electrochemical testing, all anodes underwent activation in methane at a temperature of 850 °C for a duration of one hour. Electrochemical impedance spectroscopy (EIS) was performed using an Autolab data analyzer (PGSTAT302N) at open circuit potential (OCP) across a frequency range spanning from 0.01 Hz to 100 kHz. The Zsimpwin software was utilized to determine the electrode polarization resistance (R_E) and electrode ohmic resistance (R_Ω).

3. Result and Discussion

Figure 1 illustrates the X-ray diffraction (XRD) outcomes obtained from the LFC and LFCP powders subjected to calcination at 900 °C in an air atmosphere. The XRD pattern of the LFC calcined powder displayed a close resemblance to that of $LaFe_{0.6}Co_{0.4}O_3$ (JCPDS card no. 00-044-0361), indicating the absence of any impurities. Notably, the XRD pattern of the LFCP powder exhibited a noticeable shift towards lower angles compared to that of LFC. This shift can be attributed to the reduction in interplanar distances between crystals, which occurs due to the introduction of Pd doping. Consequently, it can be inferred that LFC and LFCP perovskite structures can be formed within the porous framework of the SCM anode electrode subsequent to the impregnation of LFC and LFCP solutions.

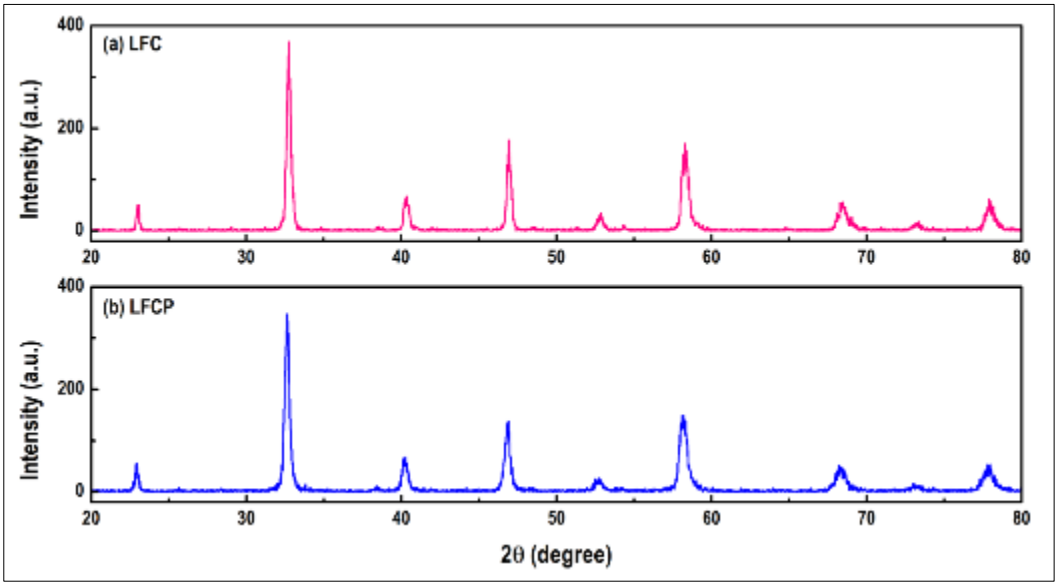

Figure 1 XRD patterns of LFC and LFCP solutions calcined at 900 °C for 2 h in air.

Figure 2 depicts the impedance spectra of a SCM anode. The measurements were carried out at OCP and various temperatures while using methane as the fuel. The impedance spectra were evaluated using an equivalent circuit denoted as $R_\Omega(R_hQ_h)(R_mQ_m)(R_lQ_l)$, wherein R_Ω signifies the ohmic resistance of the cell. Additionally, R_h, R_m, and R_l represent the polarization resistances of the electrodes ($R_E = R_h + R_m + R_l$), while Q_h, Q_m, and Q_l correspond to constant phase elements observed at high, medium, and low frequencies, respectively.

The resistance of electrode polarization during the oxidation of methane was found to be 15.81 Ω cm^2 at a temperature of 750 °C. As the temperature was increased to 800 and 850 °C, the resistance decreased to 11.91 and 7.30 Ω cm^2, respectively. The findings from the impedance spectra analysis are summarized in Table 1. To understand the different stages of the methane oxidation reaction, the activation energy for the high-, medium-, and low-frequency arcs was determined and found to be 1.04, -0.042, and 0.87 eV, respectively. These results suggest that the high- and low-frequency arcs are thermally activated, while the medium-frequency arc shows slight thermal deactivation.

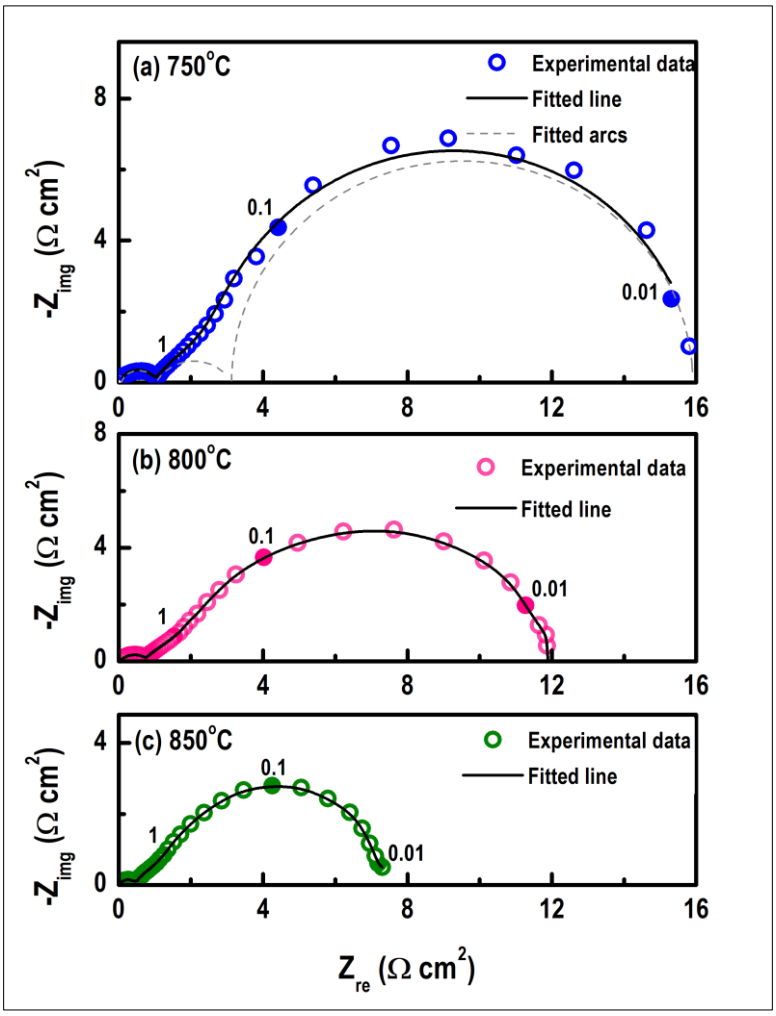

Figure 2 SCM anode electrode polarization resistance at (a) 750 (b) 800 and (c) 850 °C in methane. Points are experimental data and solid lines are fitted data with the equivalent circuit $R_\Omega(RQ)_1(RQ)_2(RQ)_3$. Dashed lines show each impedance arc. Closed symbols mark the frequency points from 0.01 Hz to 100 kHz at each frequency decade.

Table 1 Fitted impedance results for the methane oxidation reaction on the SCM anode at different temperatures

Temp (°C)	**Ohmic resistance (Ω cm²)**	**Electrode Polarization resistance**								
		High frequency arc			Medium frequency arc			Low frequency arc		
		R_1 (Ωcm²)	Q_1 (Ωcm²sⁿ)	n_1	R_2 (Ωcm²)	Q_2 (Ωcm²sⁿ)	n_2	R_3 (Ωcm²)	Q_3 (Ωcm²sⁿ)	n_3
750	4.54	0.93	5.5×10^{-4}	0.8	1.71	0.14	0.7	13.17	0.36	0.9
800	3.83	0.58	3.7×10^{-4}	0.8	1.95	0.19	0.7	9.16	0.35	0.9
850	3.15	0.29	2.9×10^{-4}	0.8	2.06	0.21	0.7	4.95	0.37	0.9

At 850 °C, the high-frequency arc exhibited a peak frequency of 2511 Hz and an activation energy of 1.04 eV. In the context of the methane oxidation reaction on the LSCM/YSZ composite anode in wet methane, Jiang et al. [63] observed three distinct impedance arcs. They attributed the high-frequency arc to the transport of charged species across the interface of LSCM/YSZ. Another study compared the $La_{0.4}Sr_{0.6}Ti_{1-x}Mn_xO_{3-\delta}$ (LSTM) anode with the LSTM/YSZ composite anode, where the latter showed a remarkably smaller high-frequency arc than the LSTM anode. The researchers concluded that the composite anode's LSTM/YSZ interface area was significantly larger, resulting in enhanced charge transfer [64]. Given the similarities between the characteristics of the high-frequency arc in this study and the findings

in the references [63, 64], it can be inferred that the high-frequency arc is associated with the transfer of charged species in the SCM anode.

Primdahl and Mogensen [65] studied the electrochemical oxidation of wet H_2 on Ni/YSZ electrode at 1000 °C in a three-electrode setup. They observed an arc with summit frequency around 1 Hz in the impedance spectra that has small negative activation energy (−0.09 eV). They attributed this arc to the gas conversion on the surface of Ni/YSZ anode electrode. In this study, the composition of fuel on the anode electrode is completely different from the counter and reference electrode side. The summit frequency of medium-frequency arc, at 850 °C, is 0.9 Hz and the activation energy of this arc is -0.042 eV. Comparison of this arc with references [64, 65], attributes the medium-frequency arc to the gas conversion on the surface of SCM anode electrode.

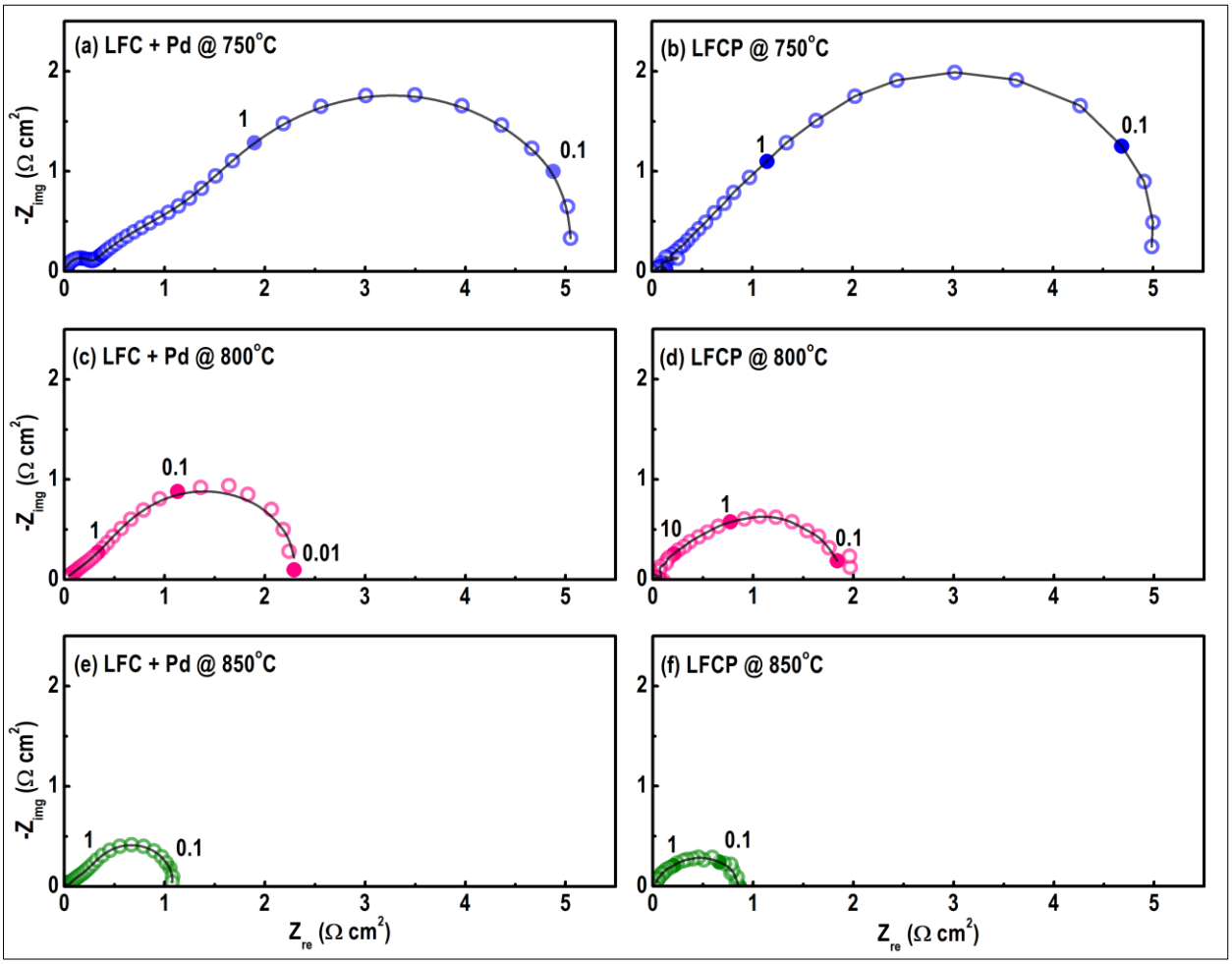

Figure 3 Impedance spectra of SCM anodes impregnated with (a, c, and e) LFC+Pd and (b, d, and f) LFCP at (a, b) 750, (c, d) 800, and (e, f) 850 °C in methane. Points are experimental data and solid lines are fitted data with the equivalent circuit $R_\Omega(R_hQ_h)(R_mQ_M)(R_lQ_l)$. Dashed lines show each impedance arc. Closed symbols mark the frequency points from 0.01 Hz to 100 kHz at each frequency decade.

The impedance spectra of a Ni/YSZ anode in a moist H_2 environment at 850 °C were investigated by Jiang et al. [66]. They discovered an arc with a peak frequency of 0.02 Hz and an activation energy of 0.42 eV, which they attributed to the process of hydrogen dissociative adsorption on Ni particles. Since the low-frequency arc is thermally activated and reaches a peak frequency of 0.87 Hz at 850 °C, it can be inferred that this arc corresponds to the hydrogen dissociative adsorption on the SCM anode electrode [66].

Figure 3 presents the impact of treating the SCM electrode with LFC+Pd and LFCP solutions on its performance under varying methane temperatures. At 750 °C, the polarization resistance of the electrode decreased from 15.81 to 5.05 and 4.98 Ω cm² after impregnation with LFC+Pd and LFCP solutions, respectively. When the temperature was raised to 800 °C, the resistance decreased from 11.91 to 2.29 and 1.96 Ω cm² for LFC+Pd and LFCP solutions, respectively. This trend continued at 850 °C, with the resistance dropping from 7.30 to 1.07 and 0.86 Ω cm² for LFC+Pd and LFCP solutions,

respectively. Across all three temperatures, LFCP demonstrated greater enhancement compared to LFC+Pd, possibly due to the heightened activity of Pd ions within the perovskite structure compared to Pd single atoms. Notably, the reduction in resistance was significantly more pronounced at 850 °C, which can be attributed to the increased catalytic activity of LFC and LFCP perovskites under high-temperature conditions.

Examining Tables 2 and 3, which present the obtained impedance outcomes concerning the methane oxidation process on both LFC+Pd and LFCP-infiltrated SCM anodes, offers additional insights for delving into the electrochemical impact of LFC+Pd and LFCP on the SCM electrode. Figure 6 portrays the influence of each solution on parameters such as electrode polarization resistance as well as the characteristic arcs at high, medium, and low frequencies.

Table 2 Fitted impedance results for the methane oxidation reaction on the SCM anode impregnated with LFC+Pd solution at different temperatures**.**

Temp (°C)	**Ohmic resistance (Ω cm²)**	**Electrode polarization resistance**								
		High frequency arc			Medium frequency arc			Low frequency arc		
		R_1 (Ωcm^2)	Q_1 ($\Omega cm^2 s^n$)	n_1	R_2 (Ωcm^2)	Q_2 ($\Omega cm^2 s^n$)	n_2	R_3 (Ωcm^2)	Q_3 ($\Omega cm^2 s^n$)	n_3
750	4.48	0.23	4.6×10^{-4}	1	1.02	0.17	0.8	3.80	0.45	0.7
800	3.79	0.18	2.9×10^{-4}	1	0.36	0.18	0.8	1.75	0.44	0.7
850	2.94	-	-	-	0.23	0.19	0.8	0.84	0.41	0.7

Table 3 Fitted impedance results for the methane oxidation reaction on the SCM anode impregnated with LFCP solution at different temperatures**.**

Temp(°C)	**Ohmic resistance (Ω cm²)**	**Electrode polarization resistance**								
		High frequency arc			Medium frequency arc			Low frequency arc		
		R_1 (Ωcm^2)	Q_1 ($\Omega cm^2 s^n$)	n_1	R_2 (Ωcm^2)	Q_2 ($\Omega cm^2 s^n$)	n_2	R_3 (Ωcm^2)	Q_3 ($\Omega cm^2 s^n$)	n_3
750	4.39	0.24	3.7×10^{-4}	0.9	0.43	0.06	1	4.31	0.37	0.8
800	3.67	0.20	3.8×10^{-4}	0.9	0.16	0.05	1	1.60	0.31	0.8
850	2.51	-	-	-	0.11	0.03	1	0.75	0.29	0.8

The electrode polarization resistance of the SCM anode in the context of methane electro-oxidation exhibited a marked decrease following the introduction of both impregnation solutions. This reduction in polarization resistance can be primarily attributed to the discernible diminution observed at medium and low frequencies. The decrease in polarization resistance at low frequencies may be attributed to the augmentation of the anode's catalytic activity towards hydrogen adsorption facilitated by the impregnation of both solutions. Moreover, in the realm of medium frequencies, the incorporation of LFCP solution led to a notable reduction in electrode polarization resistance compared to LFC+Pd solution, possibly stemming from the remarkable catalytic prowess of LFCP in facilitating methane decomposition. In contrast, when the LFC+Pd solution was employed for impregnation, a substantial reduction in electrode polarization resistance at high frequencies ensued, which is likely linked to the promotion of ionic conduction within the anode as a result of LFC+Pd solution impregnation. It can be reasonably inferred that the impregnation of LFCP exerts a significant influence across all three frequency arcs.

Figure 7 illustrates the SEM micrographs depicting the SCM anode electrode's morphological changes prior to and subsequent to impregnation with LFC+Pd and LFCP solutions. The SEM imagery distinctly reveals the emergence of nanoparticles on the surface of the SCM anode electrode upon the introduction of both impregnation solutions. Notably, the formation of LFCP nanoparticles appears more pronounced when contrasted with the outcomes observed for LFC and Pd. As previously discussed, the SCM anodes subjected to LFCP solution impregnation exhibited diminished electrode polarization resistance in comparison to those treated with LFC+Pd solution. This enhanced performance

associated with LFCP solution can be attributed to the homogeneous dispersion of LFCP nanoparticles, which are found to be well-formed within the porous framework of the SCM anode.

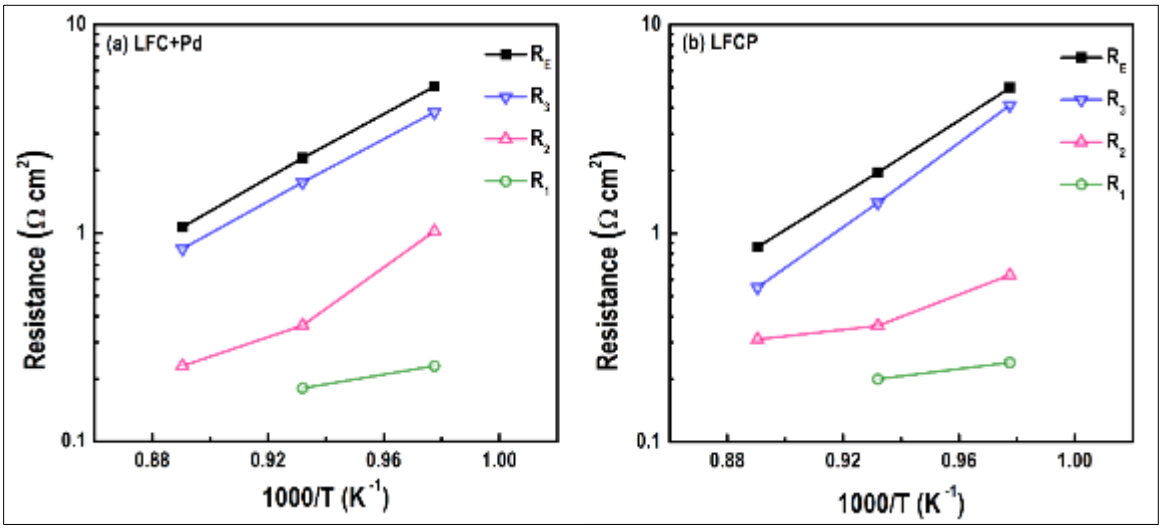

Figure 6 Effect of (a) LFC+Pd and (b) LFCP solutions impregnation on R_1, R_2, R_3, and R_E of SCM anode at 750, 800, and 850 °C in methane.

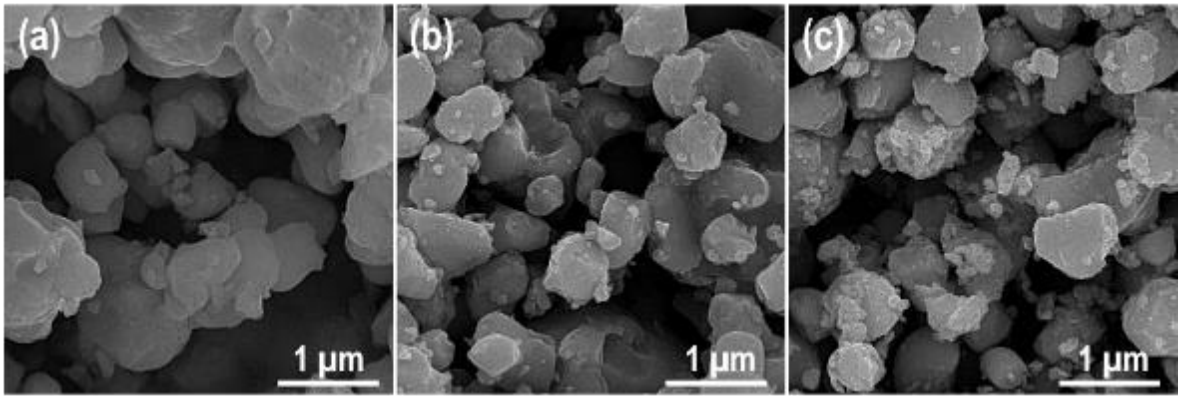

Figure 7 SEM micrograph of SCM anode electrode, (a) before, and after (b) LFC+Pd (c) and (d) LFCP solution impregnation.

4. Conclusion

SCM anode had large electrode polarization resistance for methane oxidation at 850 °C. Deconvolution of the impedance spectra by using an equivalent circuit revealed that electro-oxidation of methane on the SCM anode electrode is limited by at least three electrode processes. These processes are related to the charge transfer, at high-frequencies, gas conversion, at medium-frequencies and hydrogen dissociative adsorption on the SCM anode electrode at low-frequencies. The SCM electrode polarization resistance reduced strongly with LFC+Pd solution impregnation. LFC nanoparticles promoted the electro-catalytic property of SCM anode by facilitating the processes of methane decomposition and hydrogen adsorption. However, results revealed that doping Pd in the LFC perovskite structure promotes the electrode performance compared to metallic Pd. The electrode polarization resistance at low frequencies decreased with of LFCP solution more than LFC+Pd solution.

Compliance with ethical standards

Disclosure of conflict of interest

No conflict of interest to be disclosed.

References

[1] Rajabi R, Sun S, Billings A, Mattick VF, Khan J, Huang K. Insights into Chemical and Electrochemical Interactions between Zn Anode and Electrolytes in Aqueous Zn− ion Batteries. Journal of The Electrochemical Society. 2022;169(11):110536.

[2] Taghavi H. Liquid Cooling System for a High Power, Medium Frequency, and Medium Voltage Isolated Power Converter [M.S.]. United States -- South Carolina: University of South Carolina; 2023.

[3] Taghavi M, Gharehghani A, Nejad FB, Mirsalim M. Developing a model to predict the start of combustion in HCCI engine using ANN-GA approach. Energy Conversion and Management. 2019;195:57-69.

[4] Bhuvela P, Taghavi H, Nasiri A, editors. Design Methodology for a Medium Voltage Single Stage LLC Resonant Solar PV Inverter. 2023 12th International Conference on Renewable Energy Research and Applications (ICRERA); 2023: IEEE.

[5] Rajabi R, Sun S, Huang K, editors. Performance Comparison of Three Polymer Electrolytes for Zinc Ion Batteries. 243rd ECS Meeting with the 18th International Symposium on Solid Oxide Fuel Cells (SOFC-XVIII); 2023: ECS.

[6] Taghavi M, Perera LP, editors. Data Driven Digital Twin Applications Towards Green Ship Operations. International Conference on Offshore Mechanics and Arctic Engineering; 2022: American Society of Mechanical Engineers.

[7] Taghavi H, El Shafei A, Nasiri A, editors. Liquid Cooling System for a High Power, Medium Frequency, and Medium Voltage Isolated Power Converter. 2023 12th International Conference on Renewable Energy Research and Applications (ICRERA); 2023: IEEE.

[8] Salmasi F, Sabahi N, Abraham J. Discharge coefficients for rectangular broad-crested gabion weirs: experimental study. Journal of Irrigation and Drainage Engineering. 2021;147(3):04021001.

[9] Taghavi M, Perera LP, editors. Multiple Model Adaptive Estimation Coupled With Nonlinear Function Approximation and Gaussian Mixture Models for Predicting Fuel Consumption in Marine Engines. International Conference on Offshore Mechanics and Arctic Engineering; 2023: American Society of Mechanical Engineers.

[10] Fan L, Zhu B, Su P-C, He C. Nanomaterials and technologies for low temperature solid oxide fuel cells: recent advances, challenges and opportunities. Nano Energy. 2018;45:148-76.

[11] Soltanizade A, Babaei A, Ataie A, Seyed-Vakili SV. Temperature dependency of activity of nano-catalysts on La 0.6 Sr 0.4 Co 0.2 Fe 0.8 O 3− δ cathode of solid oxide fuel cells. Journal of Applied Electrochemistry. 2019;49:1113-22.

[12] Yang G, El Loubani M, Chalaki HR, Kim J, Keum JK, Rouleau CM, et al. Tuning Ionic Conductivity in Fluorite Gd-Doped CeO2-Bixbyite RE2O3 (RE= Y and Sm) Multilayer Thin Films by Controlling Interfacial Strain. ACS Applied Electronic Materials. 2023;5(8):4556-63.

[13] Babazadeh Dizaj R. DEVELOPMENT OF LSF-BASED DUAL-PHASE CATHODES FOR INTERMEDIATE TEMPERATURE SOLID OXIDE FUEL CELLS: Middle East Technical University; 2022.

[14] Dizaj RB, Sabahi N. Optimizing LSM-LSF composite cathodes for enhanced solid oxide fuel cell performance: Material engineering and electrochemical insights. 2023.

[15] Li H, Wang W, Wang L, Wang M, Park K-Y, Lee T, et al. Unlocking the Potential of A-Site Ca-Doped LaCo0. 2Fe0. 8O3− δ: A Redox-Stable Cathode Material Enabling High Current Density in Direct CO2 Electrolysis. ACS Applied Materials & Interfaces. 2023;15(37):43732-44.

[16] Wang M, Wu W, Lin Y, Tang W, Gao G, Li H, et al. Improved Solid-State Reaction Method for Scaled-Up Synthesis of Ceramic Proton-Conducting Electrolyte Materials. ACS Applied Energy Materials. 2023;6(15):8316-26.

[17] Lin J, Li H, Wang W, Qiu P, Tao G, Huang K, et al. Atmospheric plasma spraying to fabricate metal-supported solid oxide fuel cells with open-channel porous metal support. Journal of the American Ceramic Society. 2023;106(1):68-78.

[18] Nakhi A, Mostafa S, Karimi A, Mobli M. Unveiling the Promoted LSTM/YSZ Composite Anode for Direct Utilization of Hydrocarbon Fuels. International Journal of Science and Engineering Applications. 2023;12(12):18 - 24.

[19] Jeena M, Bok T, Kim SH, Park S, Kim J-Y, Park S, et al. A siloxane-incorporated copolymer as an in situ cross-linkable binder for high performance silicon anodes in Li-ion batteries. Nanoscale. 2016;8(17):9245-53.

[20] Rajabi R, Raghu S, James R, Huang K, Khan JA, editors. PERFORMANCE COMPARISON OF BATTERY THERMAL MANAGEMENT SYSTEMS BASED ON NUMERICAL SIMULATION. ASTFE Digital Library; 2023: Begel House Inc.

[21] Raghu S, Rajabi R, James R, Huang K, Khan JA, editors. Performance Comparison of Thermal Management Systems for Battery Packs Based on Numerical Simulation. Heat Transfer Summer Conference; 2023: American Society of Mechanical Engineers.

[22] Lee KT, Wachsman ED. Role of nanostructures on SOFC performance at reduced temperatures. Mrs Bulletin. 2014;39(9):783-91.

[23] Mobli M, Li C, editors. On the heat transfer characteristics of a single bubble growth and departure during pool boiling. International Conference on Nanochannels, Microchannels, and Minichannels; 2016: American Society of Mechanical Engineers.

[24] Park K-Y, Lee T, Wang W, Li H, Chen F. High-performance Ruddlesden–Popper perovskite oxide with in situ exsolved nanoparticles for direct CO 2 electrolysis. Journal of Materials Chemistry A. 2023;11(39):21354-64.

[25] Aminnia N, Adhav P, Darlik F, Mashhood M, Saraei SH, Besseron X, et al. Three-dimensional CFD-DEM simulation of raceway transport phenomena in a blast furnace. Fuel. 2023;334:126574.

[26] Rostaghi Chalaki H, Babaei A, Ataie A, Seyed-Vakili SV. LaFe 0.6 Co 0.4 O 3 promoted LSCM/YSZ anode for direct utilization of methanol in solid oxide fuel cells. Ionics. 2020;26:1011-8.

[27] Mobli M, Bayat M, Li C. Estimating bubble interfacial heat transfer coefficient in pool boiling. Journal of Molecular Liquids. 2022;350:118541.

[28] Mobli M, Farouk T, editors. High pressure micro glow discharge: Detailed approach to gas temperature modeling. APS Annual Gaseous Electronics Meeting Abstracts; 2014.

[29] Aminnia N, Estupinan Donoso AA, Peters B. Developing a DEM-Coupled OpenFOAM solver for multiphysics simulation of additive manufacturing process. Scipedia com. 2022.

[30] Ge XM, Chan SH, Liu QL, Sun Q. Solid oxide fuel cell anode materials for direct hydrocarbon utilization. Advanced Energy Materials. 2012;2(10):1156-81.

[31] Mahamud R, Mobli M, Farouk TI, editors. Modes of oscillation in a high pressure microplasma discharges. 2014 IEEE 41st International Conference on Plasma Sciences (ICOPS) held with 2014 IEEE International Conference on High-Power Particle Beams (BEAMS); 2014: IEEE.

[32] Mobli M, Mahamud R, Farouk T, editors. High pressure micro plasma discharge: Effect of conjugate heat transfer. 2013 19th IEEE Pulsed Power Conference (PPC); 2013: IEEE.

[33] Wang W, Li H, Vera CYR, Lin J, Park K-Y, Lee T, et al. Improving the performance for direct electrolysis of CO 2 in solid oxide electrolysis cells with a Sr 1.9 Fe 1.5 Mo 0.5 O 6− δ electrode via infiltration of Pr 6 O 11 nanoparticles. Journal of Materials Chemistry A. 2023;11(16):9039-48.

[34] Park K-Y, Lee T, Wang W, Li H, Chen F, editors. A Highly Performing Electrode with in-Situ Exsolved Nanoparticles for Direct Electrolysis of CO2. Electrochemical Society Meeting Abstracts 242; 2022: The Electrochemical Society, Inc.

[35] Aminnia N. CFD-XDEM coupling approach towards melt pool simulations of selective laser melting. 2023.

[36] Abbas HF, Daud WW. Hydrogen production by methane decomposition: a review. International journal of hydrogen energy. 2010;35(3):1160-90.

[37] Mobli M. Thermal analysis of high pressure micro plasma discharge. 2014.

[38] Wang M, Wang L-C, Li H, Wu W, Snyder SW, Gao G, et al. Nanostructured carbon as highly efficient and stable anodes for ethylene production and power generation in protonic ceramic electrochemical cells. Carbon. 2022;199:379-86.

[39] Sun R, Li H, Guan Y, Du Y, Shen H, Xu J. Crystallization Behavior and Luminescence of Inkjet Printing CH3NH3PbBr3. Crystal Research and Technology. 2021;56(8):2100004.

[40] McIntosh S, Gorte RJ. Direct hydrocarbon solid oxide fuel cells. Chemical reviews. 2004;104(10):4845-66.

[41] Chalaki HR, Babaei A, Ataie A, Seyed-Vakili S-V, editors. The Effect of Impregnation of Ceramic Nano-particles on the Performance of LSCM/YSZ Anode Electrode of Solid Oxide Fuel Cell. 5th International Conference on Materials Engineering and Metallurgy; 2016.

[42] Mobli M. Characterization Of Evaporation/Condensation During Pool Boiling And Flow Boiling: University of South Carolina; 2018.

[43] Wang W, Tang W, Ding H, Chen F, Ding D, editors. Rational Identification of Doping Strategy to Achieve a Highly Conductive and Reliable Protonic Electrolyte for Electrochemical Cells. Electrochemical Society Meeting Abstracts 239; 2021: The Electrochemical Society, Inc.

[44] Du Y, Li H, Jia X, Dou Y, Xu J, Eklund P. Preparation and thermoelectric properties of graphite/poly (3, 4-ethyenedioxythiophene) nanocomposites. Energies. 2018;11(10):2849.

[45] Jia-Yue X, Xiao-Xiao L, Min J, Hai-Bo Z, Kimura H, Hao-Yang H, et al. Growth and characterization of all-inorganic perovskite CsPbBr3 crystal by a traveling zone melting method. Journal of Inorganic Materials. 2018;33(11):1253-8.

[46] Estupinan Donoso AA, Aminnia N, Peters B, Michels A. On the Reduction of Computational Costs for Tungsten Powder Bed Processes. 2022.

[47] Aminnia N, Estupinan Donoso AA, Peters B. CFD-DEM simulation of melt pool formation and evolution in powder bed fusion process. 2022.

[48] Su C, Wang W, Liu M, Tadé MO, Shao Z. Progress and prospects in symmetrical solid oxide fuel cells with two identical electrodes. Advanced Energy Materials. 2015;5(14):1500188.

[49] Li H, Wang L, Wu W, Bian W, Ding D, Chen F, editors. C2H6 Dehydrogenation and Electrical Power Production in a Protonic Conducting Fuel Cell with in-Situ Exsolved Metal Nanoparticle Catalyst. Electrochemical Society Meeting Abstracts 239; 2021: The Electrochemical Society, Inc.

[50] Aminnia N, Peters B, ESTUPINAN AA. Multi-Scale Modeling of Melt Pool Formation and Solidification in Powder Bed Fusion: A Fully Coupled Computational Fluid Dynamics-Extended Discrete Element Method Approach. Available at SSRN 4502227.

[51] Huang Y-H, Dass RI, Xing Z-L, Goodenough JB. Double perovskites as anode materials for solid-oxide fuel cells. Science. 2006;312(5771):254-7.

[52] Li H, Wang W, Park K-Y, Lee T, Chen F, editors. A-Site Doping Effect on the Performance of Sr2Fe1. 4 Ni0. 1Mo0. 5O6-Δ Anodes for SOFCs. Electrochemical Society Meeting Abstracts 242; 2022: The Electrochemical Society, Inc.

[53] Marina OA, Canfield NL, Stevenson JW. Thermal, electrical, and electrocatalytical properties of lanthanum-doped strontium titanate. Solid State Ionics. 2002;149(1-2):21-8.

[54] dos Santos-Gómez L, León-Reina L, Porras-Vázquez J, Losilla E, Marrero-López D. Chemical stability and compatibility of double perovskite anode materials for SOFCs. Solid State Ionics. 2013;239:1-7.

[55] Huang Y-H, Liang G, Croft M, Lehtimaki M, Karppinen M, Goodenough JB. Double-perovskite anode materials Sr2MMoO6 (M= Co, Ni) for solid oxide fuel cells. Chemistry of materials. 2009;21(11):2319-26.

[56] Kumar P, Jena P, Patro P, Lenka R, Sinha A, Singh P, et al. Influence of lanthanum doping on structural and electrical/electrochemical properties of double perovskite Sr2CoMoO6 as anode materials for intermediate-temperature solid oxide fuel cells. ACS applied materials & interfaces. 2019;11(27):24659-67.

[57] Aminnia N, Shateri M, Gheibi S, Torabi F. Modeling of Two-Phase flow in the Cathode Gas Diffusion Layer to Investigate Its Effects on a PEM Fuel Cell.

[58] mahmoodreza Hashemi S, Aminnia N, Derakhshan S. Optimization Design of Pumps as Turbines (PATs) Arrays in a Water Distribution Network Aiming Energy Recovery.

[59] Shirvani SMN, Gholami M, Afrasiab H, Talookolaei RAJ. Optimal design of a composite sandwich panel with a hexagonal honeycomb core for aerospace applications. Iranian Journal of Science and Technology, Transactions of Mechanical Engineering. 2023;47(2):557-68.

[60] Seyed Mostafa Nasrollahpour Shirvani MG, Hamed Afrasiab, Ramazanali Jafari Talookolaei. Optimization of a Composite Sandwich Panel with Honeycomb Core Under Out-of-Plane Pressure with NMPSO Algorithm. The 28th Annual International Conference of Iranian Society of Mechanical Engineers (ISME)2020.

[61] Rath MK, Lee K-T. Superior electrochemical performance of non-precious Co-Ni-Mo alloy catalyst-impregnated Sr2FeMoO6-δ as an electrode material for symmetric solid oxide fuel cells. Electrochimica Acta. 2016;212:678-85.

[62] Shen J, Chen Y, Yang G, Zhou W, Tadé MO, Shao Z. Impregnated LaCo0. 3Fe0. 67Pd0. 03O3-δ as a promising electrocatalyst for "symmetrical" intermediate-temperature solid oxide fuel cells. Journal of Power Sources. 2016;306:92-9.

[63] Jiang SP, Chen X, Chan S, Kwok J, Khor K. (La0. 75Sr0. 25)(Cr0. 5Mn0. 5) O3/YSZ composite anodes for methane oxidation reaction in solid oxide fuel cells. Solid State Ionics. 2006;177(1-2):149-57.

[64] Fu Q, Tietz F, Stöver D. La0. 4Sr0. 6Ti1− x Mn x O3− δ perovskites as anode materials for solid oxide fuel cells. Journal of the Electrochemical Society. 2006;153(4):D74.

[65] Primdahl S, Mogensen M. Gas conversion impedance: a test geometry effect in characterization of solid oxide fuel cell anodes. Journal of the electrochemical Society. 1998;145(7):2431.

[66] Jiang S, Wang W, Zhen Y. Performance and electrode behaviour of nano-YSZ impregnated nickel anodes used in solid oxide fuel cells. Journal of power sources. 2005;147(1-2):1-7..